Phase-Coded FMCW for Coherent MIMO Radar

Kumbul, Utku; Petrov, Nikita ; Vaucher, Cicero S.; Yarovoy, Alexander

DOI
10.1109/TMTT.2022.3228950

Publication date
2023

Document Version
Final published version

Published in
IEEE Transactions on Microwave Theory and Techniques

Phase-Coded FMCW for Coherent MIMO Radar

Utku Kumbul, *Graduate Student Member, IEEE*, Nikita Petrov, Cicero S. Vaucher, *Senior Member, IEEE*, and Alexander Yarovoy, *Fellow, IEEE*

***Abstract*— The phase-coded linear-frequency-modulated continuous-wave (PC-FMCW) waveform with a low sampling processing strategy is studied for coherent multiple-input multiple-output (MIMO) radar. The PC-FMCW MIMO structure, which jointly uses both fast-time and slow-time coding, is proposed to reduce sidelobe levels while preserving high range resolution, unambiguous velocity, good Doppler tolerance, and low sampling needs. The sensing performance and practical aspects of the introduced PC-FMCW MIMO structure are evaluated theoretically and verified experimentally. The numerical simulations and experiments demonstrate that the proposed MIMO keeps the advantages of the linear-frequency-modulated continuous-wave (LFMCW) waveform, including computational efficiency and low sampling demands, while having the ability to provide low sidelobe levels with simultaneous transmission.**

***Index Terms*— Linear frequency modulation (LFM), multiple-input multiple-output (MIMO), phase-modulated chirps, radar signal processing.**

I. Introduction

THE multiple-input multiple-output (MIMO) systems are commonly used in automotive radars for detection, tracking, and classification of targets in traffic environments under diverse weather conditions [1]. The MIMO technology enables achieving high angular resolution while keeping the radar complexity and costs low. To implement the MIMO schemes, it is essential that the waveform of different transmitters can be identified upon signal reception. Therefore, the transmitted waveforms should be orthogonal or have very low cross-correlations.

In this study, we investigate the utilization of the phase-coded linear-frequency-modulated continuous wave (PC-FMCW) waveforms with a low sampling receiving strategy for simultaneous MIMO transmission. We propose a novel PC-FMCW MIMO radar structure, which combines both fast-time and slow-time coding to lower sidelobes while maintaining simultaneous transmission of the waveforms, high range resolution, unambiguous velocity, good Doppler tolerance, and low signal sampling requirements. Furthermore, for the first time in literature, we assess the performance of such waveforms in application to coherent MIMO radar. To do that, we overview the state-of-the-art MIMO techniques in Section II and then introduce the signal model and possible receiver structures for the single transmit scenario with PC-FMCW waveform in Section III. Then in Section IV, we give the signal model and the required processing steps for the proposed PC-FMCW MIMO radar with a simultaneous transmission scheme. Subsequently, the performance of the proposed MIMO radar is assessed in different domains and compared with the other state-of-the-art techniques in Section V. Moreover, we have applied the proposed method to a real scenario, and the experimental verification is demonstrated in Section VI. Finally, the conclusions are drawn in Section VII.

Manuscript received 23 September 2022; revised 17 November 2022; accepted 1 December 2022. Date of publication 21 December 2022; date of current version 5 June 2023. This work was supported in part by the TU Delft Industry Partnership Program (TIPP), which is funded by NXP Semiconductors N.V. and Holland High Tech Systems and Materials, through the Project Coded Radar for Interference Suppression in Super-Dense Environments (CRUISE) under Grant TKIHTSM/18.0136. *(Corresponding author: Utku Kumbul.)*

Utku Kumbul and Alexander Yarovoy are with the Microwave Sensing, Systems and Signals (MS3) Group, Faculty of Electrical Engineering, Mathematics and Computer Science, Delft University of Technology, 2628 CD Delft, The Netherlands (e-mail: u.kumbul@tudelft.nl).

Nikita Petrov and Cicero S. Vaucher are with NXP Semiconductors N.V., 5656 AG Eindhoven, The Netherlands, and also with the Department of Microelectronics, Delft University of Technology, 2628 CD Delft, The Netherlands.

Color versions of one or more figures in this article are available at https://doi.org/10.1109/TMTT.2022.3228950.

Digital Object Identifier 10.1109/TMTT.2022.3228950

II. State-of-the-Art MIMO Techniques

Currently, there are two competing waveform classes for the MIMO systems in automotive radars: phase-modulated continuous wave (PMCW) and linear-frequency-modulated continuous wave (LFMCW) [1]. While the PMCW waveforms can provide high mutual orthogonality to realize the MIMO radar [2], [3], [4], they requires high sampling from analog-to-digital converter (ADC) to achieve high range resolution [5]. Moreover, the PMCW waveform has poor Doppler tolerance, and the orthogonality between codes heavily suffers from the Doppler frequency shift due to the target's movement [6]. On the other hand, the LFMCW waveforms can provide high range resolution, good Doppler tolerance, and low sidelobes [7], [8], [9]. Moreover, simple hardware implementation and low sampling requirements from ADC favor the utilization of the LFMCW waveforms in the automotive radars [5]. However, these advantages come with the price of having limited waveform diversity. Without additional techniques to secure orthogonality, the multiple LFMCW radars operating simultaneously within the same frequency bandwidth suffer from mutual interference [10], [11], [12], [13]. To ensure orthogonality between transmitters, various transmitting schemes have been proposed for the LFMCW waveforms [14]. These methods aim to achieve orthogonality between transmitters in time, frequency, chirp slope, or code domains, which result in different advantages and disadvantages.

The simplest approach to distinguish the received signals associated with different transmitters is time-division multiple

access (TDMA). In the TDMA transmission scheme, chirp sequences are consecutively transmitted one by one by each transmit antenna. However, the time duration between chirps transmitted by the same antenna (pulse repetition interval) increased, and hence the maximum unambiguous velocity of the target is degraded by a factor of the number of transmitters [1]. Moreover, different transmitters illuminate a target at different time instances, which introduces a phase error for moving targets and increases the angle estimation errors [15]. To deal with this, various techniques are proposed to eliminate the phase migration introduced by every moving target in the virtual array response [15], [16], [17]. Although the motion-induced phase error can be addressed, reducing the maximum unambiguous velocity by a factor of transmit channels prevents increasing the number of transmitters, and thus improving the angular resolutions is limited in the TDMA transmission scheme.

Another method to achieve orthogonality between transmitting channels is slow-time code division multiple access (ST-CDMA). In the ST-CDMA transmission scheme, the phase codes are used to modulate the initial phases of each chirp pulse and let all the transmit channels simultaneously transmit signals with different codes. One particular implementation of such coding is achieved using Doppler-division multiple access (DDMA). In the DDMA transmission scheme, the phase shifts are set such that different transmit channels appear in different parts of the Doppler spectrum, and thus they emulate Doppler frequency shift [18]. However, sharing the Doppler spectrum downgrades the maximum unambiguous velocity by a factor of the number of transmit channels. Consequently, a target with a velocity higher than the reduced maximum unambiguous velocity will appear in the Doppler spectrum assigned to another transmit channel. This disadvantage restrains increasing the number of transmitters and thus limits improving the angular resolution using DDMA. In general ST-CDMA implementations, the phase codes are designed to spread signals of different transmitters throughout the full Doppler spectrum as pseudonoise after decoding in the slow time with the reference phase code signal. As a result, a maximum of $10\log_{10}(N_p)$ dB isolation between transmitter channels in slow time can be achieved using N_p chirp pulses [19]. However, decoding in the slow time leads to increased sidelobes in the Doppler domain. Moreover, the code length and the number of chirp pulses are limited for the slow-time phase coding [14]. Hence, the slow-time phase coding alone is not enough to provide high mutual orthogonality and suffers from high Doppler sidelobes.

In addition, the fast-time code division multiple access (FT-CDMA) can provide high mutual orthogonality between transmitting channels to realize simultaneous transmission for the MIMO system. Consequently, the FT-CDMA transmission scheme can address the degradation problem in the maximum unambiguous velocity seen in the TDMA and DDMA transmission schemes. For this purpose, the circulating codes which use a small frequency shift are proposed to modulate LFMCW waveforms in adjacent frequency bands [20]. On the other hand, such coding results in degradation in the range resolution. Alternatively, the circulating codes are used with slow-time coding for the pulses in [21]. However, this method requires a special technique for Doppler processing, and the windowing function cannot be applied to reduce sidelobes further. In [22], the chirp signal modulated with orthogonal frequency division multiplexing (OFDM) waveform is proposed to improve the range resolution. However, such a waveform imposes different limitations on the waveform parameter selection and is difficult to use.

The aforementioned limitations can be circumvented using the PC-FMCW waveform. In the PC-FMCW radar, the phase-coded signals are used to modulate the phase changes within the chirp, and a maximum of $10\log_{10}(N_c)$ dB isolation between transmitted signals can be achieved in the fast time using N_c number of chips per chirp. Such PC-FMCW waveform keeps all the benefits of the LFMCW waveform, such as good Doppler tolerance and high range resolution, while providing high mutual orthogonality necessary for the simultaneous MIMO transmission [23]. Moreover, the PC-FMCW waveforms can be jointly used with the slow-time coding to decrease the sidelobe levels further.

Recently, various processing methods for the PC-FMCW waveforms have been developed [24], [25], [26], [27], [28], [29], [30]. Initially, the traditional full-band match filter receiver, where the received signal is correlated with the transmitted signal, is used to process such waveforms [24]. However, the acquisition of the received signals with its full band demands a high sampling rate from ADC. To reduce the sampling requirements, two approaches based on the dechirping receiver structure have been proposed: the compensated stretch processing and the group delay filter [25], [26], [27], [28], [29], [30]. The compensated stretch processing corresponds to performing a filter bank for all ranges of interest, which requires high computational complexity compared with the standard stretch processing. The group delay filter, on the other hand, can be efficiently realized via an infinite impulse response (IIR) filter [30]. Thus, the limited processing power of automotive radars favors the utilization of the group delay filter receiver. However, the group delay filter causes a quadratic phase shift on the dechirped signal and distorts the received code signal. Consequently, this distortion significantly degrades the decoding performance when codes with a high number of phase changes per chirp (meaning substantial code bandwidth) are used [31]. Such performance degradation limits the code length and, associated with it, signal isolation. To deal with this issue, the phase smoothing operation is proposed to obtain smoothed phase code (e.g. Gaussian minimum shift keying), and then the phase lag compensation (PLC) is applied to the transmitted phase code to eliminate the undesired effect of the group delay filter [32].

III. Preliminaries

This section introduces the preliminary studies for the PC-FMCW waveforms and the competing receiver approaches with low sampling requirements.

Assume a radar transmits multiple chirp pulses with a chirp duration T and chirp bandwidth B. The fast-time term t can be defined as $t = t' - mT$, where $t \in [0,\ T]$, $m = 0, \ldots, N_p - 1$ is

the index of slow time, N_p is the number of chirp pulses, and t' is the total duration of the one snapshot or frame. In only fast-time coding case, each chirp pulses use the same phase-coded signal $s(t)$ to modulate chirp phases. Then, the mth phase-coded chirp in the transmitted burst can be given as

$$x_{\mathrm{T}}(t,m) = s(t)e^{-j(2\pi f_c t+\pi k t^2)} \tag{1}$$

where f_c is the carrier frequency and $k = B/T$ is the chirp slope. Herein, the phase of the chirp signal changes according to the code sequence $s(t)$. Subsequently, the chip (code) duration is defined by $T_c = T/N_c$, where N_c denotes the number of chips within one chirp. Increasing N_c raises the bandwidth of the code as $B_c = N_c/T$. In this study, we assume that the bandwidth of $s(t)$ is much smaller than the chirp bandwidth $B_c \ll B$. The transmitted signal (1) is reflected from a target and received with a delay. The round trip delay for a target with constant velocity can be written as

$$\tau(t,m) = \frac{2(R_0 + v_0(t+mT))}{c} = \tau_0 + \frac{2v_0}{c}(t+mT) \tag{2}$$

where R_0 is the range, v_0 is the velocity, and c is the speed of light. Then, the received signal reflected from a point-like target is the round trip delayed version of the transmitted signal and can be written as

$$x_{\mathrm{R}}(t,m) = \alpha_0\, x_{\mathrm{T}}(t-\tau(t,m),m) \tag{3}$$

where α_0 is a complex amplitude proportional to the target backscattering coefficient and propagation effects. Hereafter, we substitute all the constant terms of signal processing into α_0 without loss of generality. In the dechirping process, the received signal is mixed with the complex conjugate of the uncoded chirp signal. Then, the dechirped signal can be written as [31]

$$\begin{aligned} x_{\mathrm{M}}(t,m) &= x_{\mathrm{R}}(t,m)e^{j(2\pi f_c t+\pi k t^2)} \\ &= \alpha_0 s(t-\tau(t,m))e^{j(2\pi f_c\tau_0+2\pi(f_b+f_d)t+2\pi f_d mT)} \\ &\approx \alpha_0 s(t-\tau_0)e^{j(2\pi f_b t+2\pi f_d mT)} \end{aligned} \tag{4}$$

where $f_b = k\tau_0$ is the beat frequency, $f_d = 2v_0 f_c/c$ is the Doppler frequency, and we used $(1 - 2v_0/c) \approx 1$ since the target velocities $v_0 \ll c$ for automotive scenario. Moreover, $2\pi f_c\tau_0$ is incorporated into α_0 as a constant phase term. In addition, the Doppler frequency shift in the fast time is typically negligible compared with the beat frequency resolution (one range cell) for dechirping-based automotive radar processing, and thus we can approximate $2\pi(f_b + f_d)t \approx 2\pi f_b t$. Note that the Doppler frequency shift in the slow-time $2\pi f_d mT$ will be used for velocity estimation via slow-time processing. The slow-time processing is straightforward and the same as in the traditional FMCW automotive radar processing. The filter bank and group delay receiver techniques are only related to the fast-time processing part, and thus we focus on signal analysis in the fast time for Sections III-A–III-C. The dechirped signal related to the fast-time part can be recast as

$$x_{\mathrm{M}}(t) = \alpha_0\, s(t-\tau_0)e^{j(2\pi f_b t)}. \tag{5}$$

A. Filter Bank Receiver

The matched filter, which is an optimal receiver in white noise, can be realized by performing a filter bank for all possible range–Doppler hypotheses [33]. To apply filter bank, we can alternatively interpret the formulation of (5) by considering the response of a general waveform $s(t)$ with the time delay τ_0 and the virtual Doppler frequency shift $f_{\mathrm{VD}} = k\tau_0$. Herein, the direct relationship between the parameters pair $f_{\mathrm{VD}} = k\tau_0$ necessitates a 1-D search across the parameter τ. Then for each τ, the filter bank receiver performs [31]

$$y(\tau) = \int_0^T x_{\mathrm{M}}(t)s^*(t-\tau)e^{-j(2\pi k\tau t)}dt. \tag{6}$$

After sampling by ADC operating at the sampling frequency f_s and stored in a vector, the complex mixer output can be defined as

$$\mathbf{x}_{\mathrm{M}} = \alpha_0 s(n/f_s - \tau_0)e^{j(2\pi k\tau_0 n/f_s)} \tag{7}$$

where $\mathbf{x}_{\mathrm{M}} \in \mathbb{C}^{N\times 1}$ and $t = n/f_s, n = 0,\ldots,N-1$.

For each given τ, the hypothesis part in the integral (6) can be written via a Hadamard product of two vectors $\mathbf{b}(\tau)\odot\mathbf{s}(\tau)$

$$\begin{aligned} \mathbf{b}(\tau) &= e^{j(2\pi k\tau n/f_s)} \\ \mathbf{s}(\tau) &= s(n/f_s - \tau) \end{aligned} \tag{8}$$

where $\mathbf{b}(\tau), \mathbf{s}(\tau) \in \mathbb{C}^{N\times 1}, n = 0,\ldots,N-1$. Then, the vectors with different τ are stacked up in columns and stored in the $N \times N_r$ matrices as $\mathbf{B} = [\mathbf{b}(\tau_0),\ldots,\mathbf{b}(\tau_{N_r})]$ and $\mathbf{S} = [\mathbf{s}(\tau_0),\ldots,\mathbf{s}(\tau_{N_r})]$, where the number of range cells in the range grid is denoted by N_r. Subsequently, the convolution (6) can be represented via a vector product as

$$\mathbf{y} = (\mathbf{B}\odot\mathbf{S})^H\mathbf{x}_{\mathrm{M}}. \tag{9}$$

Consequently, the vector $\mathbf{y}$ contains the range profile. In [25], shifting the reference phase-coded signal for each range hypothesis is called compensation, and this receiver is called compensated stretch processing. Performing the filter bank receiver approach causes the computational complexity of discrete Fourier transform (DFT) $\mathcal{O}(N^2)$. A more efficient implementation via fractional Fourier transform has been recently proposed, hence being still more costly than the group delay filter receiver [34], [35].

B. Group Delay Filter Receiver (Without PLC)

The group delay filter receiver approach aims to align the signals from all ranges for decoding the phase-coded signal first and then apply fast Fourier transform (FFT) for extracting the range information from the beat signal. This alignment in fast time can be realized by applying the group delay filter before decoding as initially proposed in [29], [30]. Such filter leads to the group delay $\tau_{\mathrm{g}}(f)$, which shifts the envelope of the signal and equals to the first derivative of the filter phase response [32]. In this case, the group delay filter should eliminate τ_0, and hence the desired group delay can be written as

$$\tau_{\mathrm{g}}(f)\big|_{f=f_b} = -\frac{1}{2\pi}\frac{d\theta(f)}{df}\bigg|_{f=f_b} = -\tau_0 = -f_b/k. \tag{10}$$

Subsequently, the group delay filter, which gives the desired group delay in (10), can be found as [32]

$$H_{\mathrm{g}}(f) = e^{j\left(\frac{\pi f^2}{k}\right)}. \tag{11}$$

The resulting group delay filter is applied to the dechirped signal given in (5) by multiplying its spectrum. Note that the group delay filter applies different time delays to each frequency component to eliminate delay term τ_0 for each coded beat signal. As a result of applying nonlinear frequency shifts, the group delay filter creates an unwanted dispersion effect on the phase-coded signal. This dispersion term can be written as

$$H_{\mathrm{dis}}(f) = e^{j\left(\frac{\pi}{k}(f-f_b)^2\right)}. \tag{12}$$

Then, the dechirped signal in the time domain becomes

$$y_{\mathrm{o}}(t) = \alpha_0(s(t) \otimes h_{\mathrm{dis}}(t))e^{j(2\pi f_b t)} \tag{13}$$

where $\otimes$ denotes the convolution operation. For decoding, the dechirped signal is multiplied with the complex conjugate of the reference code signal $s^*(t)$. However, the nonlinear shift on the spectrum of the code signal leads to convolution with $h_{\mathrm{dis}}(t)$. Consequently, the decoding becomes imperfect, and the decoded signal can be written as [32]

$$\begin{aligned} y_{\mathrm{d}}(t) &= y_{\mathrm{o}}(t)s^*(t) \\ &= \alpha_0 e^{j(2\pi f_b t + \epsilon(t))} \end{aligned} \tag{14}$$

where $(\cdot)^*$ denotes the complex conjugate, and $\epsilon(t)$ represents the residual phase error due to the imperfection in decoding. The range profile can be obtained by performing FFT on the decoded signal, and thus the group delay filter receiver leads to the computational complexity of FFT $\mathcal{O}(N\log_2(N))$. However, the imperfection in decoding leads to distortion of the range profile. Moreover, the group delay dispersion effect becomes crucial for a phase-coded signal with a wide spectrum. Hence, the sidelobe levels increase significantly as the bandwidth of modulation sequence $s(t)$ raises [32]. To improve the decoding performance, compensation of the group delay dispersion effect will be discussed in Section III-C.

C. PLC for Group Delay Filter Receiver

The group delay dispersion effect can be eliminated by performing the PLC on the transmitted phase-coded signal before transmission [32]. The required PLC filter is the complex conjugate of the dispersion term and can be written as

$$H_{\mathrm{lag}}(f) = e^{-j\left(\frac{\pi f^2}{k}\right)}. \tag{15}$$

The resulting PLC filter is performed to the spectrum of the transmitted code. Then the dechirped signal given in (5) becomes

$$x_{\mathrm{M}}(t) = \alpha_0 \hat{s}(t-\tau_0)e^{j(2\pi f_b t)} \tag{16}$$

where $\hat{(\cdot)}$ denotes the phase-coded signals that are modified after performing a PLC filter. Subsequently, the group delay filter (11) is applied to the spectrum of (16), and the resulting signal in the time domain becomes [32]

$$y_{\mathrm{o}}(t) = \alpha_0 s(t)e^{j(2\pi f_b t)}. \tag{17}$$

Note that each coded beat signal is perfectly aligned, and the group delay dispersion effect is eliminated using PLC. After applying the decoding, the decoded signal becomes

$$y_{\mathrm{d}}(t) = \alpha_0 e^{j(2\pi f_b t)}. \tag{18}$$

It can be seen in (18) that the beat signals are recovered properly. This helps reuse all the software algorithms previously developed for the LFMCW radar. In addition, large code bandwidth, which is essential to achieve high orthogonality, can be used without degrading the sidelobe levels. It should be noted that PLC leads to an amplitude variation in the transmitted waveform [32].

IV. Proposed PC-FMCW MIMO

This section applies the introduced waveform and processing steps given in [32] to the MIMO system and provides the signal model for both fast-time and slow-time coded PC-FMCW. The block diagram of the proposed MIMO radar structure is illustrated in Fig. 1.

Assume an MIMO radar simultaneously transmits the PC-FMCW waveforms, in which each chirp pulse uses different phase lag compensated codes for both the fast-time and slow-time coding. The transmitted waveform for the pth transmitter can be written as

$$x_{\mathrm{T}_p}(t,m) = \hat{s}_{p,m}(t)e^{-j\left(2\pi f_c t + \pi k t^2\right)} \tag{19}$$

where $1 \le p \le P$ is the index of the transmitter, m is the index of the chirp sequence, P is the number of transmitters, and $\hat{s}_{p,m}(t)$ is the phase-coded signal modified by a PLC filter. Here, the transmitted codes need to be orthogonal with each other for the mth chirp pulse and pth transmitter. Consider the MIMO system has L number of receiving antenna elements, and the index of the receiver is represented as $1 \le l \le L$. The received signal at the lth receiver will be the round trip delayed version of the transmitted signal at the pth transmitter. The received signal reflected from a moving point-like target can be represented as

$$x_{\mathrm{R}_l}(t,m) = \alpha_0\, a_{\mathrm{R}_l}(\theta) \sum_{p=1}^{P} a_{\mathrm{T}_p}(\theta) x_{\mathrm{T}_p}(t-\tau(t,m),m) \tag{20}$$

where $a_{\mathrm{T}_p}(\theta)$ and $a_{\mathrm{R}_l}(\theta)$ are obtained from the steering vectors of the transmitter and receiver antennas, respectively, and can be written as

$$a_{\mathrm{T}_p}(\theta) = e^{j2\pi d_t(p-1)\frac{\sin(\theta)}{\lambda}} \tag{21}$$

and

$$a_{\mathrm{R}_l}(\theta) = e^{j2\pi d_r(l-1)\frac{\sin(\theta)}{\lambda}} \tag{22}$$

where d_t and d_r are the spacing between transmitters and receivers, respectively.

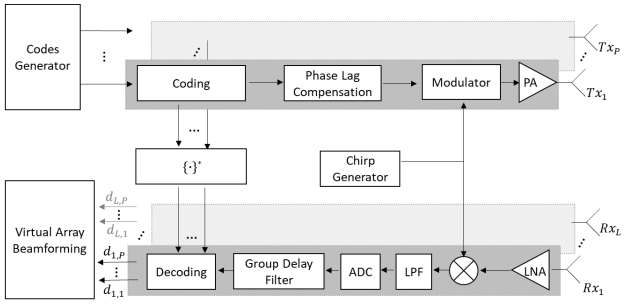

Fig. 1. Block diagram of the proposed MIMO radar.

To get the beat signals, each received signal is mixed with the complex conjugate of the uncoded chirp signal as shown in (4). Then, the dechirped signals can be represented as

$$\begin{aligned} x_{\mathrm{M}_l}(t,m) &= x_{\mathrm{R}_l}(t,m)e^{j\left(2\pi f_c t+\pi k t^2\right)} \\ &= \alpha_0 a_{\mathrm{R}_l}(\theta)\sum_{p=1}^{P} a_{\mathrm{T}_p}(\theta)\hat{s}_{p,m}(t-\tau_0)e^{j(2\pi f_b t+2\pi f_d mT)}. \end{aligned} \tag{23}$$

Applying group delay filter eliminates the τ_0 term in code signals as explained in Section III, and the resulting signal at the lth receiver becomes [32]

$$x_{\mathrm{G}_l}(t,m) = \alpha_0 a_{\mathrm{R}_l}(\theta)\sum_{p=1}^{P} a_{\mathrm{T}_p}(\theta)s_{p,m}(t)e^{j(2\pi f_b t+2\pi f_d mT)}. \tag{24}$$

Subsequently, we can apply the decoding signal for each chirp pulse, which is the complex conjugate of the transmitted code. After applying decoding in each receiver channel, the decoding output signal at the lth receiver decoded with code signal at the pth transmit channel can be obtained as

$$d_{l,p}(t,m) = x_{\mathrm{G}_l}(t,m)s^*_{p,m}(t). \tag{25}$$

After decoding, the code term is removed properly for the beat signals matched to the transmitted code. As a consequence, the beat signal matched to the transmitted signal is obtained similar to the dechirped signal of the conventional LFMCW radar, while beat signals coming from other transmitters remain coded and suppressed. Moreover, this can be used to mitigate the mutual interference between multiple radars. For orthogonal transmit channels, the virtual array with $Q = P \times L$ number of elements can be formed by stacking the decoding output signals and stored in a vector as

$$\boldsymbol{y}(t,m,q) = \begin{bmatrix} d_{1,1}(t,m) \\ \vdots \\ d_{L,1}(t,m) \\ \vdots \\ d_{1,P}(t,m) \\ \vdots \\ d_{L,P}(t,m) \end{bmatrix} \tag{26}$$

where $1 \le q \le Q$ is the index of the virtual array. From (26), we can retrieve the range, Doppler, and angle information of the target by performing a spectral analysis such as 3-D FFT.

V. Performance Assessment and Limitations

This section provides the performance assessment and limitations of the proposed PC-FMCW MIMO radar. For the numerical simulations, we consider an automotive radar operating with a carrier frequency $f_c = 77$ GHz has three transmit and four receive channels with antenna spacing $d_t = 2\lambda$ and $d_r = \lambda/2$ in the transmit and receiver subarrays, respectively. Subsequently, the virtual array of the MIMO system has 12 elements with $\lambda/2$ spacing. Moreover, we assume the transmitters and receivers operate in a linear mode. For each transmit channel, we use a chirp signal with the chirp duration $T = 25.6$ μs and the chirp bandwidth $B = 300$ MHz is coded in both slow time and fast time with the phase-coded signal. The Gaussian minimum shift keying (GMSK) is used to modulate the phase-coded signal $s(t)$, and the 3-dB bandwidth of the Gaussian filter (smoother bandwidth) is set to two times the chip bandwidth [32]. Moreover, we use the random code sequences and perform PLC before transmission for each GMSK phase-coded signal. For the fast-time coding, we use $N_c = 1024$ number of chips per chirp. The duration of the chip T_c is controlled with the number of chips per chirp as $T_c = T/N_c$, and thus the code bandwidth becomes $B_c = 40$ MHz for $N_c = 1024$. Moreover, $N_p = 255$ number of chirp pulses are transmitted for Doppler processing and slow-time coding, where each chirp uses a different phase lag compensated code signal $\hat{s}(t)$.

On the receiver side, the dechirped signals (23) are low-pass-filtered with the cutoff frequency $f_{\mathrm{cut}} = \pm 40$ MHz and sampled with $f_s = 80$ MHz. As a consequence, we have $N = 2048$ range cells (fast-time samples) for this setting. The group delay filter is applied to the sampled signal to align the beat signals of different targets. Before decoding, the same low-pass filter (LPF) is applied to the reference phase-coded signal that is used for decoding to prevent a signal mismatch. To focus on the sensing performance, we assume a noise-free scenario with a single target at the range $R_0 = 200$ m, with a radial velocity $v_0 = 10$ m/s and a target angle $\theta = 20°$. As explained in Section III, the investigated receivers perform different techniques for range processing. For each receiver technique, we apply 80-dB Chebyshev window in the range domain before processing. The Doppler and angle processing parts are the same for all the processing approaches, and we apply 60-dB Chebyshev window in both the Doppler and angle domains before taking their FFT, respectively. In addition, we normalize all the figures by the maximum value.

A. Sensing Performance

The sensing performance of the proposed MIMO radar is assessed using the investigated processing method given in Section IV and compared with the state-of-the-art processing techniques: filter bank and group delay filter without PLC.

Firstly, we investigate the sensing performance of the proposed MIMO in range, Doppler and angle domains. In Fig. 2, we simulate the range–Doppler profile of the proposed MIMO radar. It can be seen that the target response follows the main lobe in the vicinity of the target. Outside of this region, the signal returns from the simultaneously transmitted channels spread over range and Doppler cells as a noise-like pattern

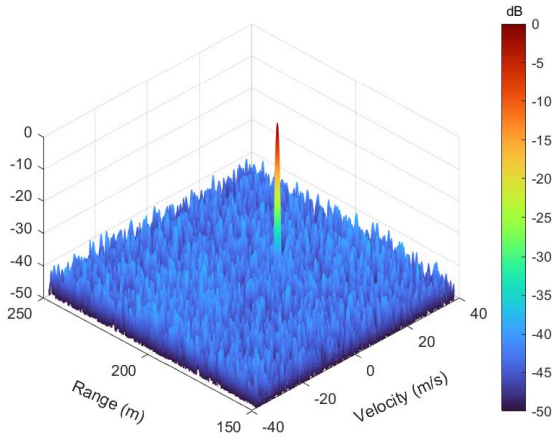

Fig. 2. Range–Doppler profile for the proposed MIMO with $N_c = 1024$ and $N_p = 255$: $R = 200$ m, $v = 10$ m/s, and $\theta = 20°$.

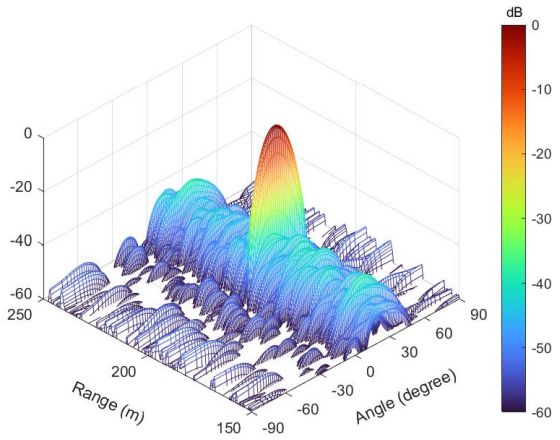

Fig. 3. Range–angle profile for the proposed MIMO with $N_c = 1024$ and $N_p = 255$: $R = 200$ m, $v = 10$ m/s, and $\theta = 20°$.

due to both the fast-time and slow-time coding. The mutual orthogonality between simultaneously transmitted channels is determined by $10\log_{10}(N_c)$ in the fast-time coding and $10\log_{10}(N_p)$ in the slow-time coding. Therefore, the theoretical limit of this suppression combined with the suppression in both slow time and fast time is 54 dB on average for perfectly orthogonal code. However, random phase coding causes a (pseudo) noise-like behavior, and the sidelobe level is altering over the range–Doppler with a peak sidelobe level (PSL) around ~ -40 dB. The PSL of a signal is determined by the maximum amplitude outside of the main lobe in a given domain. We demonstrate the range–angle profile in Fig. 3 and the velocity–angle profile in Fig. 4. Both the figures show that the target at 20° has around ~ -56-dB PSL in the angle domain while having noise-like sidelobes in the range and Doppler domains. To highlight the angular coverage performance of the proposed MIMO radar, we simulate the received target angle versus the beamforming angle (Fig. 5). Herein, the strong line along the diagonal axis indicates that beamforming can be achieved without ambiguity between simultaneously transmitted channels.

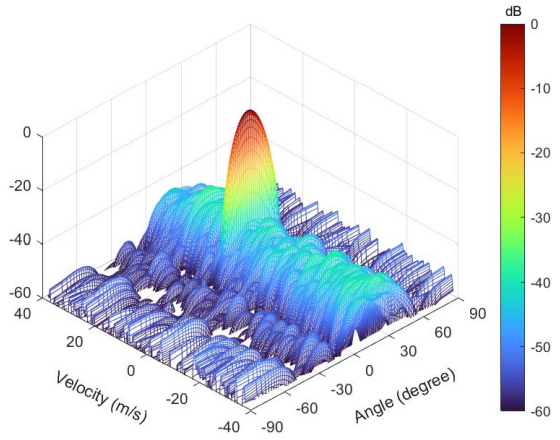

Fig. 4. Velocity–angle profile for the proposed MIMO with $N_c = 1024$ and $N_p = 255$: $R = 200$ m, $v = 10$ m/s, and $\theta = 20°$.

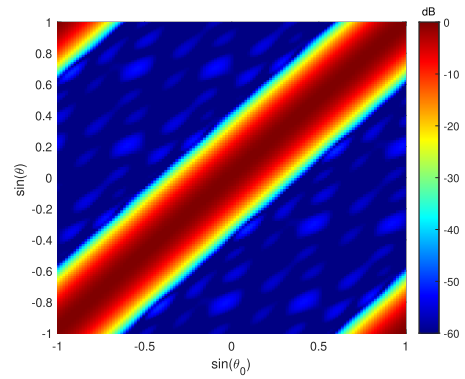

Fig. 5. Target angle versus beamforming angle for the proposed MIMO with $N_c = 1024$ and $N_p = 255$: $R = 200$ m and $v = 10$ m/s.

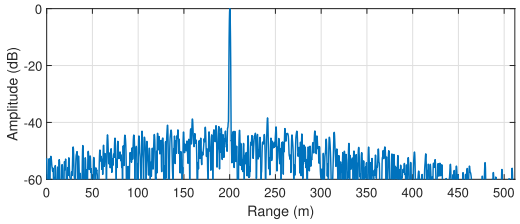

Fig. 6. Range profile of the proposed MIMO for $N_c = 1024$, $N_p = 255$, $R = 200$ m, $v = 10$ m/s, and $\theta = 20°$.

Afterward, we evaluated the sidelobe level of the proposed MIMO radar as a function of chip numbers for fast-time coding and compared it with other approaches. Since the sidelobes in the range and Doppler have a (pseudo) noise-like pattern, we consider integrated sidelobe level (ISL) as a performance metric. Moreover, the sidelobes in the range spread as a Gaussian shape due to GMSK coding (Fig. 6). Therefore, we only take into account ISL in the interval noted as $[z_1, z_4]$. Then ISL in a particular domain can be defined as [36]

$$\mathrm{ISL} = 10\log_{10}\left(\frac{\int_{z_1}^{z_2}|X(z)|^2dz + \int_{z_3}^{z_4}|X(z)|^2dz}{\int_{z_2}^{z_3}|X(z)|^2dz}\right) \quad (27)$$

where the interval $[z_2, z_3]$ defines the main lobe of a signal denoted as $X(z)$. In the numerical simulations, we consider

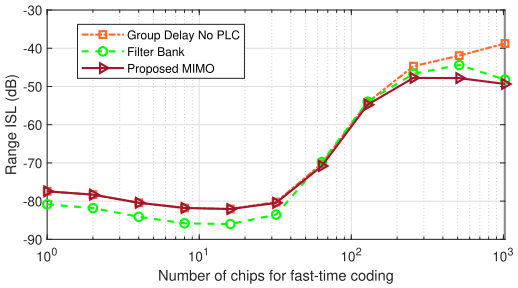

Fig. 7. Range ISL versus number of chips for fast-time coding: $N_p = 255$, $R = 200$ m, $v = 10$ m/s, and $\theta = 20°$.

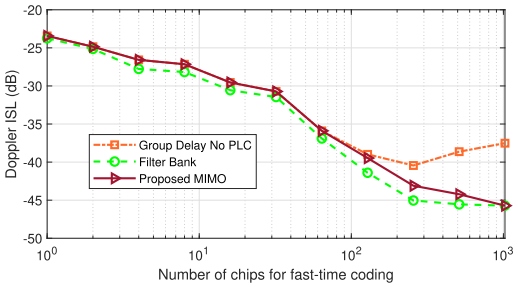

Fig. 8. Doppler ISL versus number of chips for fast-time coding: $N_p = 255$, $R = 200$ m, $v = 10$ m/s, and $\theta = 20°$.

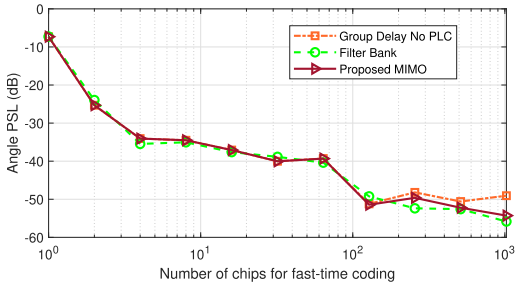

Fig. 9. Angle PSL versus number of chips for fast-time coding: $N_p = 255$, $R = 200$ m, $v = 10$ m/s, and $\theta = 20°$.

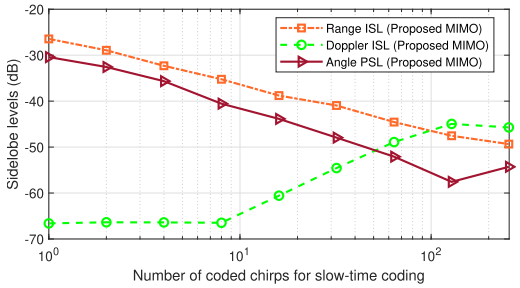

Fig. 10. Sidelobe levels of the proposed MIMO versus number of coded chirps for slow-time coding: $N_c = 1024$, $R = 200$ m, $v = 10$ m/s, and $\theta = 20°$.

the range ISL in the interval [150, 250] m and the Doppler ISL in the interval [5, 15] m/s, corresponding to the code bandwidth $\pm 0.1\ B_c$ and the unambiguous velocity $\pm 0.125\ v_{\text{un}}$, respectively, for the selected system parameters.

The range ISL and Doppler ISL of the proposed MIMO radar are compared and illustrated as a function of fast-time code length in Figs. 7 and 8, respectively. Similarly, we demonstrate the angle PSL as a function of fast-time code length in Fig. 9. It can be seen in Fig. 7 that all the investigated approaches have around ~ -80-dB range ISL for $N_c = 1$ case. When increasing the number of chips for fast-time coding, we observe that the proposed MIMO and the group delay filter without PLC provide similar performance up to $N_c = 128$, which is equivalent to $B_c = 5$ MHz for the chosen system parameters. Thereafter, the group delay filter without PLC suffers from the dispersion effect, and its sensing performance is downgraded substantially. On the other hand, the range ISL of the filter bank and proposed MIMO start to decrease and improve for the long code scenarios. Moreover, the proposed MIMO is computationally more efficient $\mathcal{O}(N \log_2(N))$ than the filter bank approach $\mathcal{O}(N^2)$ and provides the best sensing performance. Note that $N_p = 255$ chirps are still used for the slow-time coding in all the three cases. Consequently, the Doppler ISL of the three investigated approaches is around ~ -23 dB for $N_c = 1$.

To investigate the trade-offs of slow-time coding, we use fixed chips for fast-time coding $N_c = 1024$ and illustrate the sidelobe levels of the proposed MIMO as a function of the number of coded chirp pulses in Fig. 10. Here, the joint utilization of slow-time coding helps reduce sidelobe levels in range and angle with the price of increased sidelobe levels in Doppler. In particular, the proposed MIMO can achieve -49 dB range ISL, -45 dB Doppler ISL, and -54 dB angle PSL using $N_c = 1024$ chips for fast-time coding and $N_p = 255$ chirp pulses for slow-time coding. It is important to note that all the three investigated approaches use dechirping-based receivers and lower ADC sampling requirements compared with full-band matched filtering. As mentioned earlier, the suppression level improves as the number of chips for the fast-time coding raises. However, this also increases the sampling requirements for ADC as the code bandwidth B_c raises. Since we use ADC with a sampling frequency 80 MHz, we increase the number of chips for fast-time up to $N_c = 1024$, which results in $B_c = 40$ MHz. To the best of our knowledge, this ADC sampling is the limit of the current generation of automotive radars. By increasing the ADC sampling rate, higher code bandwidth, i.e., more chips for fast-time coding, can be used to improve suppression.

B. Doppler Tolerance

Next, we investigate the Doppler tolerance of the proposed MIMO radar. As explained in the introduction, the PMCW waveform suffers from Doppler frequency shift and often requires special techniques to compensate its poor Doppler tolerance [6]. However, using the chirp signal as a carrier shears the resulting ambiguity function of the phase-coded signal, i.e., the resulting ambiguity function's Doppler axis is changed to a linear combination of the Doppler frequency shift and delay [37]. Thus, the PC-FMCW waveforms have good Doppler tolerance similar to the LFMCW waveforms [23]. To demonstrate the Doppler tolerance of the proposed MIMO radar, we simulate the range ISL and angle PSL as a function of radial velocity in Figs. 11 and 12, respectively. In these simulations, we consider the scenario with $N_c = 1024$ number of chips for the fast-time coding and $N_p = 255$ pulses for the slow-time coding. It can be seen that the range ISL of the proposed MIMO radar is not affected by the Doppler shift,

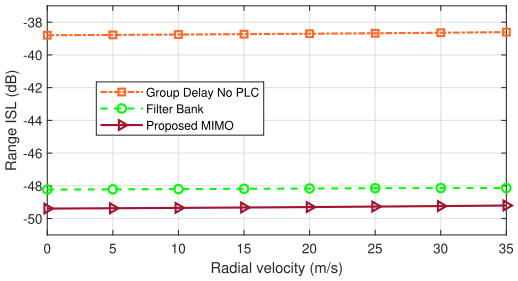

Fig. 11. Range ISL versus radial velocity: $N_c = 1024$, $N_p = 255$, $R = 200$ m, and $\theta = 20°$.

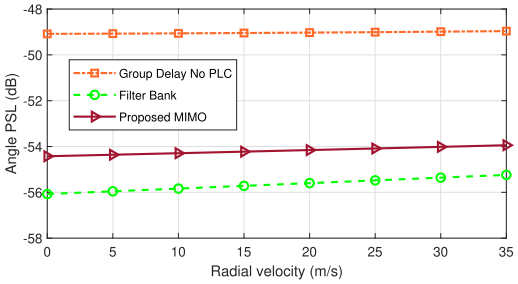

Fig. 12. Angle PSL versus velocity: $N_c = 1024$, $N_p = 255$, $R = 200$ m, and $\theta = 20°$.

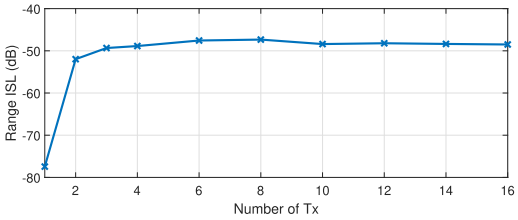

Fig. 13. Range ISL for the proposed MIMO versus the number of transmitters: $N_c = 1024$, $N_p = 255$, $R = 200$ m, $v = 10$ m/s, and $\theta = 20°$.

while the angle PSL degraded only half dB from $v = 0$ to $v = 35$ m/s. Consequently, the PC-FMCW waveforms processed with all the three investigated approaches provide good Doppler tolerance.

C. Limitations

In this section, we analyze the various limitation criteria for the proposed MIMO radar.

1) Number of Transmitters: First, we investigate the range ISL as a function of the number of transmitters as shown in Fig. 13, where we consider $N_c = 1024$ chips for the fast-time coding and $N_p = 255$ pulses for the slow-time coding. It can be observed that only one transmitter case has around ~ -80 dB range ISL. This is expected because there is no other waveform to interfere with the transmitted signal, and the receiver can provide a high dynamic range after decoding with the reference code. However, the reflected signals coming from the other transmitters act as interferers in the simultaneously transmitted MIMO system and are spread over the range–Doppler profile due to coding. As a result, the range ISL rapidly goes to -50 dB in the MIMO case. Thereafter, we observe that adding a transmitter does not significantly increase the range ISL for the chosen system parameters. Thus, a higher number of transmitters can be used

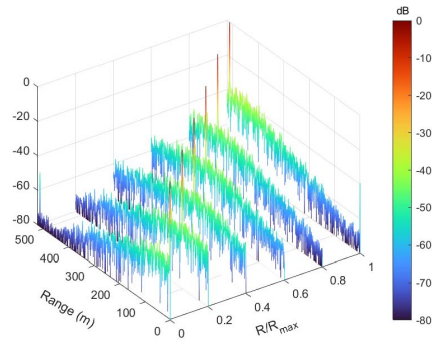

Fig. 14. Range profile for the proposed MIMO as a function of the maximal range: $N_c = 1024$, $N_p = 255$, $v = 10$ m/s, and $\theta = 20°$.

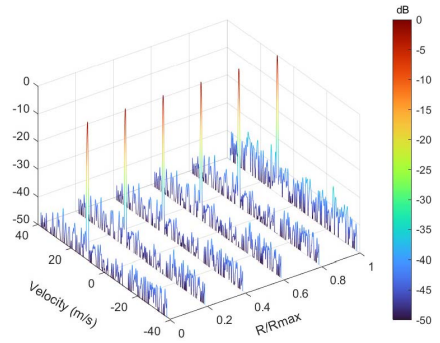

Fig. 15. Doppler profile for the proposed MIMO as a function of the maximal range: $N_c = 1024$, $N_p = 255$, $v = 10$ m/s, and $\theta = 20°$.

in other applications based on the system requirements, such as the unambiguous velocity.

2) Maximal Range: The maximal range is determined as $R_{\max} = (cf_{b_{\max}}/2k)$, and the maximum beat signal is defined by the ADC sampling as $f_{b_{\max}} = f_s/2$. We investigate the range profile as a function of the maximal range in Fig. 14, where we increase the target range for each of the six profiles plotted in the figure. Herein, we use $f_s = 80$ MHz and $B_c = 40$ MHz (for $N_c = 1024$) so that $B_c/f_s = 1/2$. Similarly, we demonstrate the velocity and angle profiles as a function of the maximal range in Figs. 15 and 16, respectively. It can be observed that the sidelobe levels are raised in the range, velocity, and angle profiles as the range of the target approaches the maximal range. This is due to the fact that the corresponding coded beat signal approaches the cutoff frequency of LPF (determined by the ADC sampling frequency) as the target range goes close to the maximal range, and hence some part of the coded beat signal spectrum is rejected by the low-pass filter of the receiver before decoding. Such filtering of the spectrum leads to imperfect decoding and downgrades the sensing performance. Therefore, the ADC sampling rate and its comparison to code bandwidth B_c/f_s have an impact on the sensing performance and should be considered in the system design. However, the range sidelobe level in the case of MIMO is mainly determined by cross correlation between the transmitted signals and thus has a minor dependency on the range, when compared with operation with a single transmitter [32].

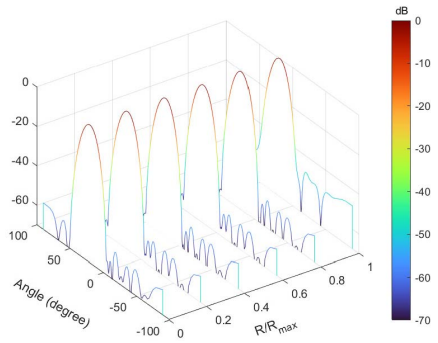

Fig. 16. Angle profile for the proposed MIMO as a function of the maximal range: $N_c = 1024$, $N_p = 255$, $v = 10$ m/s, and $\theta = 20°$.

TABLE I
EXPERIMENT SYSTEM PARAMETERS

Chirp bandwidth	B	200 MHz
Chirp duration	T	102.4 μs
Intermediate frequency	f_{IF}	300 MHz
Local oscillator	f_{LO}	9.7 GHz
Reference clock	f_{clk}	10 MHz
Carrier frequency	f_c	9.4 GHz
Wavelength	λ	0.032 m
ADC sampling frequency	f_{ADC}	40 MHz
Number of chips	N_c	1024
Chip duration	T_c	0.1μs
Chip bandwidth	B_c	10 MHz
Number of pulse	N_p	512
Number of receivers	N_{Rx}	1
Number of transmitters	N_{Tx}	4
Spacing between transmit elements	d_t	1.25λ

D. Further Discussion on MIMO Schemes

In this section, we compare the sensing performance of the proposed MIMO radar with commonly used state-of-the-art MIMO techniques. For this purpose, we demonstrate and compare the range–Doppler profiles of different MIMO schemes with the proposed MIMO radar in Fig. 17, where we used $N_p = 1024$ number of chips for fast-time coding and $N_p = 255$ number of chirps for slow-time coding. Note that the maximum unambiguous velocity $v_{\mathrm{un}} = \lambda/(4T) = 38$ m/s for a chosen system parameters. It can be seen that the maximum unambiguous velocity is degraded by a factor of $P = 3$ and becomes $v_{\mathrm{un}} = 12.6$ m/s with the TDMA transmission scheme due to an increase in the time duration between chirps transmitted by the same antenna [Fig. 17(a)]. Similarly, the same target appears at other Doppler spectrum associated with different transmitters, and the maximum unambiguous velocity is degraded by a factor of $P = 3$ with the DDMA transmission scheme as shown in Fig. 17(b). Hence, this disadvantage restrains increasing the number of transmitters and improving the angular resolution with the TDMA and DDMA transmission schemes. The slow-time coding with FMCW and the fast-time coding with PC-FMCW overcome this degradation problem in the maximum unambiguous velocity and provide $v_{\mathrm{un}} = 38$ m/s. However, the slow-time coding with FMCW suffers from high sidelobe levels in the Doppler domain, while the fast-time coding with PC-FMCW suffers from high sidelobe levels in the range domain [Fig. 17(c) and (d)] On the other hand, we observe that the proposed MIMO radar structure addresses the aforementioned limitations and achieves sidelobe levels below 40 dB in the range–Doppler profile without degrading the maximum unambiguous velocity or range resolution [Fig. 17(e)]. Thus, the proposed MIMO radar structure can be used to achieve high angular resolution and good sensing performance.

VI. EXPERIMENTS

This section demonstrates the experimental verification of the proposed MIMO structure. Since the experimental validation of the PC-FMCW waveforms is not possible with the currently available automotive radars, we use the ASTAP radar system to demonstrate the proof of concept regarding the cross-isolation between simultaneously transmitted PC-FMCW waveforms and beamforming on transmit. The ASTAP radar system consists of arbitrary waveform generator (AWG) Keysight M82190A, oscilloscope (Agilent Tech. DSO-X 91604A), up–down converters (RF amplifiers and mixers) and series-fed antenna patch array. This radar system architecture can support multiple-input single-output (MISO) configuration with multiple transmit channels and a single receiver channel. It should be noted that there is no principal difference in operation between MIMO and MISO regarding the beamforming on transmit [38]. In this experiment, we choose the system parameters as given in Table I and use 4 transmit channels to demonstrate the proof of concept. We use the GMSK phase coding with $N_c = 1024$ random code sequences for fast-time coding, and each chirp pulse uses a different random phase code signal for slow-time coding. Then, we perform PLC for each phase code signal and use $N_p = 512$ chirp pulses. The block diagram of the radar system used in the measurements is shown in Fig. 18. Herein, the radio frequency and microwave subsystems inside the up- and downconverters produce different distortions for each transmit channel. Without any calibration, such distortion downgrades the sensing performance. Thus, the frequency response of the system transfer function is measured for each channel with test measurement. Then, the inverse of the corresponding transfer functions is applied to the spectrum of the waveform in each channel to compensate the system effect and do the calibration method as discussed in [39]. After calibration, AWG produces the resulting PC-FMCW waveforms at an intermediate frequency (IF). Then, the analog IF signals in each channel are upconverted to the radio frequency (RF) using a common local oscillator (LO). Subsequently, the resulting waveforms in each channel are simultaneously transmitted via multiple series-fed patch antenna array for coherent MISO transmission. On the receiver side, the reflected signals are captured by the single receive antenna and downconverted to IF. The received IF signal is recorded by the oscilloscope, which is synchronized with AWG using a reference clock. The recorded digital data are then processed by the introduced steps given in Section IV.

For the measurements, the resulting waveforms in each channel are simultaneously transmitted to detect two moving targets (triangular reflectors are attached to pendulums), as illustrated in Fig. 19. Herein, both the pendulums are

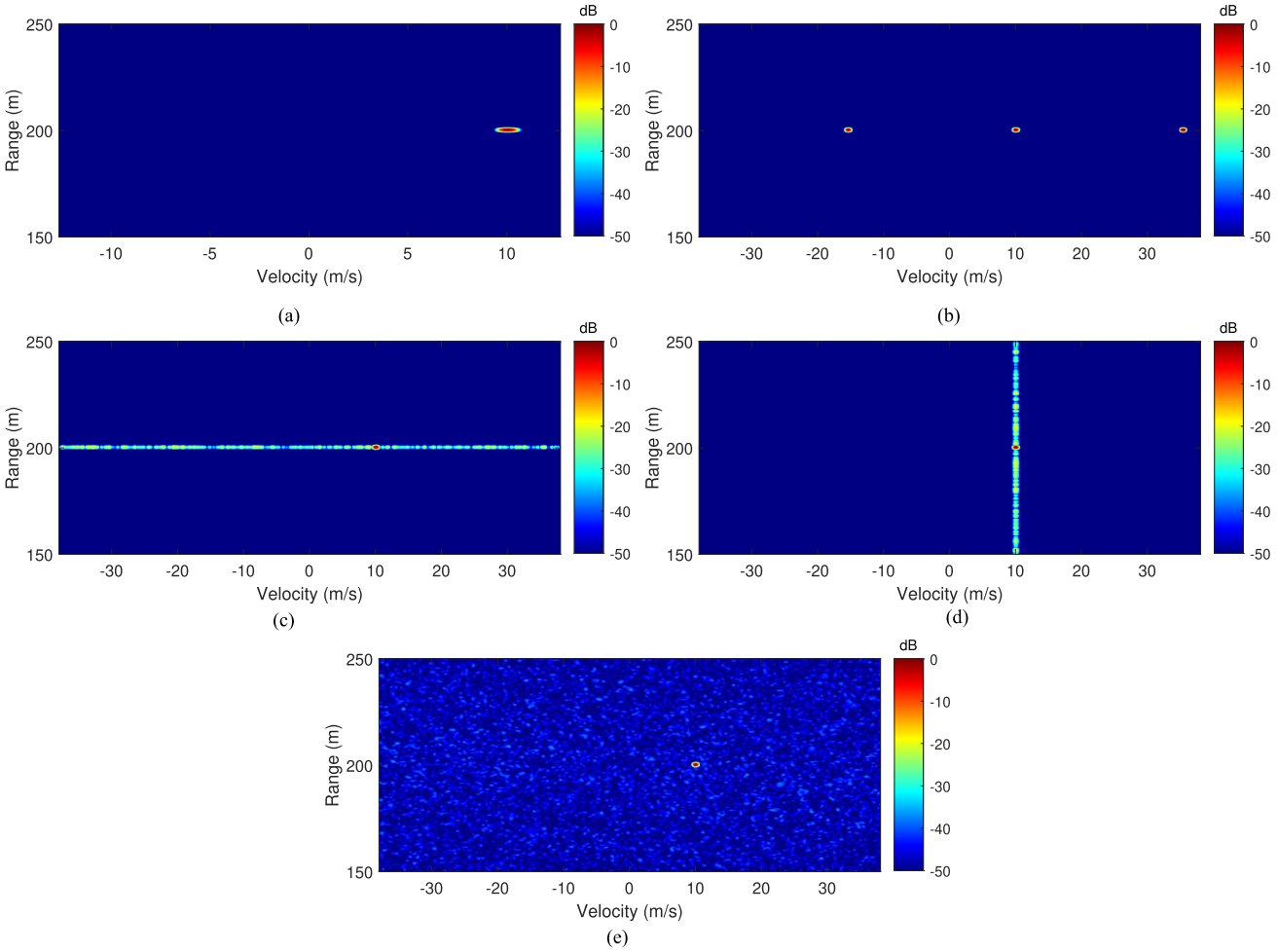

Fig. 17. Comparison of the range–Doppler profiles for different MIMO schemes. (a) TDMA FMCW. (b) DDMA FMCW. (c) ST-CDMA FMCW. (d) FT-CDMA PC-FMCW. (e) Proposed MIMO ($N_c = 1024$, $N_p = 255$, $R = 200$ m, $v = 10$ m/s, and $\theta = 20°$).

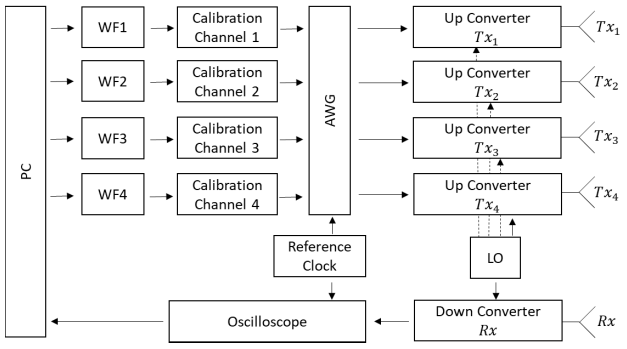

Fig. 18. Block diagram of the radar system used in the measurements.

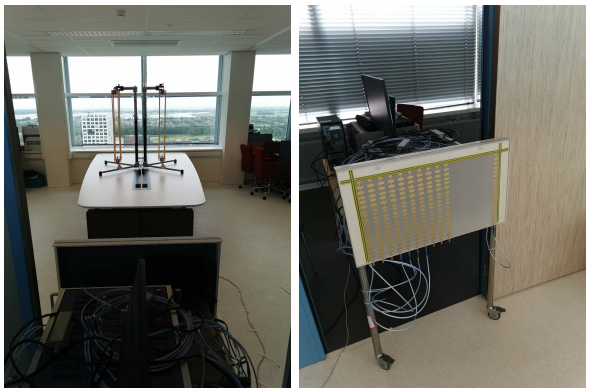

Fig. 19. Illustration of the experimental setup and antennas.

located 3.15 m away from the antenna, but one is on the left and the other is on the right compared with the antenna array boresight. During experiments, we collect the data when one pendulum moves toward the radar and the other moves away from the radar. To process the collected data, we apply the group delay filter and decoding with the reference transmitted codes for each channel as explained in Section IV. Moreover, we apply Hamming windowing in range and Doppler to highlight the sensing performance. Since the angular resolution is limited due to the available MISO configuration, we perform rectangular windowing in the angle domain. In addition, we estimate the noise level from the target-free Doppler cells and use it to normalize the processed signal power.

After processing the received data and taking 3-D FFT over range, Doppler, and angle domains, the incoherent summation over the angle domain is performed on the processed data to obtain the range–Doppler profile as shown in Fig. 20. We observe that the two moving targets appear along with the clutter in the experimental environment. The peak location

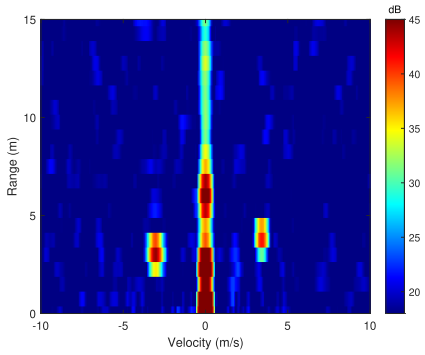

Fig. 20. Experimental result: Range–Doppler profile for two moving pendulums.

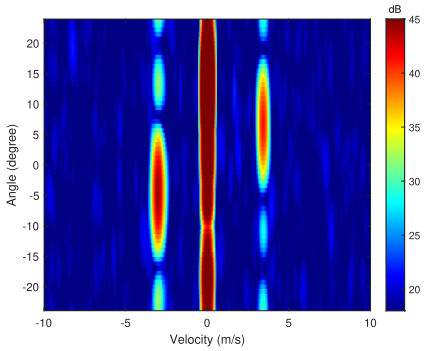

Fig. 21. Experimental result: Angle–velocity profile for two moving pendulums.

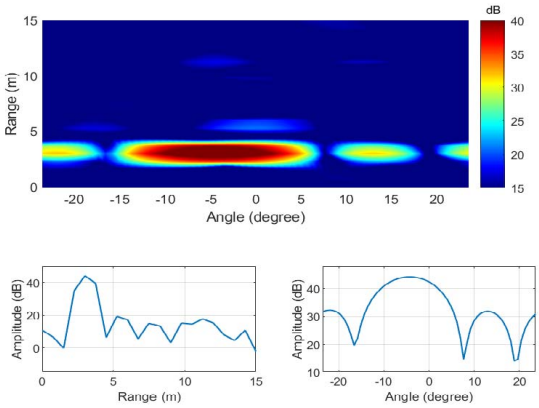

Fig. 22. Experimental result: Range–angle profile for the first pendulum.

of the first moving target is obtained at $R_1 = 3$ m with radial velocity $v_1 = -3.04$ m/s, and the peak location of the second moving target is obtained at $R_2 = 3.34$ m with radial velocity $v_2 = 3.75$ m/s. Likewise, the velocities of two moving targets can be seen in Fig. 21, where the corresponding angle–velocity map of the range cell having the maximum power is illustrated. Note that the fast-time and slow-time coding spread the power of simultaneously transmitted waveforms over the range–Doppler profile, and thus the sidelobes act like pseudorandom noise as explained in Section V. Then, we take $v_1 = -3.04$ m/s cut from the 3-D processed data and demonstrate the range–angle profile of the first moving target in Fig. 22. It can be seen that the target is obtained at $\theta_1 = -4°$ with the ∼44-dB power. Similarly, we take $v_2 = 3.75$ m/s cut from the 3-D processed data and show the range–angle

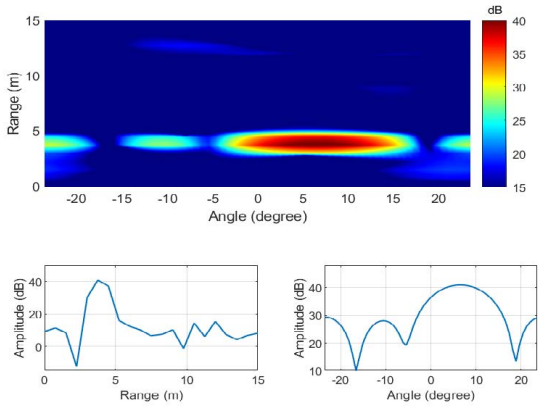

Fig. 23. Experimental result: Range–angle profile for the second pendulum.

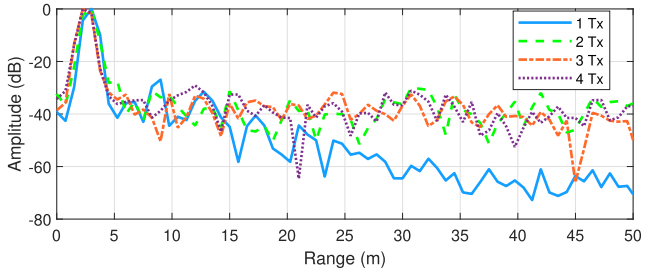

Fig. 24. Experimental result: range profiles by different numbers of transmitters.

profile of the second moving target in Fig. 23. We observe that the second target is slightly far away from the radar and obtained at $\theta_2 = 6.19°$ with the ∼41-dB power. Consequently, the experimental results verify that the proposed approach has the ability to distinguish the simultaneously transmitted signals reflected from the moving targets at different angles.

Finally, we investigate the sensing performance by different numbers of transmit channels. We consider only one moving target for all the cases. Each scenario corresponds to different measurements, and thus range varies slightly. The normalized responses of the target corresponding to different numbers of transmitters are shown in Fig. 24. One can observe that the sidelobe levels in the range profiles are similar for all the multiple transmitter scenarios and remain stable with increasing transmit channels.

VII. Conclusion

A novel PC-FMCW MIMO radar structure, based on dechirping and decoding receiving strategy to keep the low intermediate signal bandwidth, has been proposed to address the current limitations in the state-of-the-art solutions. PLC of the transmitted waveforms is used to improve the decoding performance (avoid the quadratic phase shift after group delay filter), and phase codings in both fast time and slow time are jointly used to reduce the sidelobe levels. The performance assessment of phase lag compensated PC-FMCW waveforms for MIMO applications and the practical limitations on the system design of the introduced MIMO structure are analyzed numerically and verified experimentally for the first time. Both the numerical simulations and experimental results verify that the proposed MIMO structure can combine the benefits of

LFMCW waveforms, such as high range resolution, unambiguous velocity, good Doppler tolerance, low ADC sampling requirement, and computational efficiency, with the capability of achieving low sidelobe levels in the range–Doppler–azimuth domains for simultaneous transmission. Consequently, the introduced system can be effectively used by automotive radar sensors to mitigate mutual interference between multiple radars and enhance the sensing performance of coherent MIMO transmission.

ACKNOWLEDGMENT

The authors thank Pascal Aubry and Peter Swart for their support during the experiments. They also thank the anonymous reviewers for their constructive comments that improved the quality of this article significantly.

REFERENCES

[1] S. Sun, A. P. Petropulu, and H. V. Poor, "MIMO radar for advanced driver-assistance systems and autonomous driving: Advantages and challenges," *IEEE Signal Process. Mag.*, vol. 37, no. 4, pp. 98–117, Jul. 2020.

[2] A. Bourdoux, U. Ahmad, D. Guermandi, S. Brebels, A. Dewilde, and W. Van Thillo, "PMCW waveform and MIMO technique for a 79 GHz CMOS automotive radar," in *Proc. IEEE Radar Conf. (RadarConf)*, May 2016, pp. 1–5.

[3] S. A. Hassani, A. Guevara, K. Parashar, A. Bourdoux, B. van Liempd, and S. Pollin, "An in-band full-duplex transceiver for simultaneous communication and environmental sensing," in *Proc. Asilomar Conf. Signals, Syst., Comput. (ASILOMAR)*, Oct. 2018, pp. 1389–1394.

[4] A. Bourdoux and M. Bauduin, "PMCW waveform cross-correlation characterization and interference mitigation," in *Proc. 17th Eur. Radar Conf. (EuRAD)*, Jan. 2021, pp. 164–167.

[5] F. Roos, J. Bechter, C. Knill, B. Schweizer, and C. Waldschmidt, "Radar sensors for autonomous driving: Modulation schemes and interference mitigation," *IEEE Microw. Mag.*, vol. 20, no. 9, pp. 58–72, Sep. 2019.

[6] J. Overdevest, F. Jansen, F. Uysal, and A. Yarovoy, "Doppler influence on waveform orthogonality in 79 GHz MIMO phase-coded automotive radar," *IEEE Trans. Veh. Technol.*, vol. 69, no. 1, pp. 16–25, Jan. 2020.

[7] S. D. Blunt and E. L. Mokole, "Overview of radar waveform diversity," *IEEE Aerosp. Electron. Syst. Mag.*, vol. 31, no. 11, pp. 2–42, Nov. 2016.

[8] I. Bilik, O. Longman, S. Villeval, and J. Tabrikian, "The rise of radar for autonomous vehicles: Signal processing solutions and future research directions," *IEEE Signal Process. Mag.*, vol. 36, no. 5, pp. 20–31, Sep. 2019.

[9] S. M. Patole, M. Torlak, D. Wang, and M. Ali, "Automotive radars: A review of signal processing techniques," *IEEE Signal Process. Mag.*, vol. 34, no. 2, pp. 22–35, Mar. 2017.

[10] S. Alland, W. Stark, M. Ali, and M. Hegde, "Interference in automotive radar systems: Characteristics, mitigation techniques, and current and future research," *IEEE Signal Process. Mag.*, vol. 36, no. 5, pp. 45–59, Sep. 2019.

[11] S. Neemat, O. Krasnov, and A. Yarovoy, "An interference mitigation technique for FMCW radar using beat-frequencies interpolation in the STFT domain," *IEEE Trans. Microw. Theory Techn.*, vol. 67, no. 3, pp. 1207–1220, Mar. 2019.

[12] C. Aydogdu et al., "Radar interference mitigation for automated driving: Exploring proactive strategies," *IEEE Signal Process. Mag.*, vol. 37, no. 4, pp. 72–84, Jul. 2020.

[13] U. Kumbul, F. Uysal, C. S. Vaucher, and A. Yarovoy, "Automotive radar interference study for different radar waveform types," *IET Radar, Sonar Navigat.*, vol. 16, no. 3, pp. 564–577, Mar. 2022. [Online]. Available: https://ietresearch.onlinelibrary.wiley.com/doi/abs/10.1049/rsn2.12203

[14] H. Sun, F. Brigui, and M. Lesturgie, "Analysis and comparison of MIMO radar waveforms," in *Proc. Int. Radar Conf.*, Oct. 2014, pp. 1–6.

[15] J. Guetlein, S. Bertl, A. Kirschner, and J. Detlefsen, "Switching scheme for a FMCW-MIMO radar on a moving platform," in *Proc. 9th Eur. Radar Conf.*, Oct. 2012, pp. 91–94.

[16] D. Zoeke and A. Ziroff, "Phase migration effects in moving target localization using switched MIMO arrays," in *Proc. 12th Eur. Radar Conf. (EuRAD)*, Sep. 2015, pp. 85–88.

[17] J. Bechter, F. Roos, and C. Waldschmidt, "Compensation of motion-induced phase errors in TDM MIMO radars," *IEEE Microw. Wireless Compon. Lett.*, vol. 27, no. 12, pp. 1164–1166, Dec. 2017.

[18] F. Jansen, "Automotive radar Doppler division MIMO with velocity ambiguity resolving capabilities," in *Proc. 16th Eur. Radar Conf.*, Oct. 2019, pp. 245–248.

[19] P. Wang, P. Boufounos, H. Mansour, and P. V. Orlik, "Slow-time MIMO-FMCW automotive radar detection with imperfect waveform separation," in *Proc. IEEE Int. Conf. Acoust., Speech Signal Process. (ICASSP)*, May 2020, pp. 8634–8638.

[20] G. Babur, P. Aubry, and F. Le Chevalie, "Simple transmit diversity technique for phased array radar," *IET Radar, Sonar Navigat.*, vol. 10, no. 6, pp. 1046–1056, Jun. 2019. [Online]. Available: https://ietresearch.onlinelibrary.wiley.com/doi/abs/10.1049/iet-rsn.2015.0311

[21] S. Li, L. Zhang, N. Liu, J. Zhang, and S. Tang, "Transmit diversity technique based on joint slow-time coding with circulating code," *IET Radar, Sonar Navigat.*, vol. 11, no. 8, pp. 1243–1250, Aug. 2017. [Online]. Available: https://ietresearch.onlinelibrary.wiley.com/doi/abs/10.1049/iet-rsn.2016.0595

[22] D. Schindler, B. Schweizer, C. Knill, J. Hasch, and C. Waldschmidt, "MIMO-OFDM radar using a linear frequency modulated carrier to reduce sampling requirements," *IEEE Trans. Microw. Theory Techn.*, vol. 66, no. 7, pp. 3511–3520, Jul. 2018.

[23] U. Kumbul, N. Petrov, C. S. Vaucher, and A. Yarovoy, "Sensing performance of different codes for phase-coded FMCW radars," in *Proc. 19th Eur. Radar Conf. (EuRAD)*, Sep. 2022, pp. 1–4.

[24] J. Reneau and R. R. Adhami, "Phase-coded LFMCW waveform analysis for short range measurement applications," in *Proc. IEEE Aerosp. Conf.*, Mar. 2014, pp. 1–6.

[25] P. M. McCormick, C. Sahin, S. D. Blunt, and J. G. Metcalf, "FMCW implementation of phase-attached radar-communications (PARC)," in *Proc. IEEE Radar Conf. (RadarConf)*, Apr. 2019, pp. 1–6.

[26] F. Uysal, "Phase coded frequency modulated continuous wave radar system," NL Patent 2020050066 W, Aug. 13, 2020.

[27] F. G. Jansen, F. Laghezza, and F. Lampel, "Radar-based communication," U.S. Patent 11 204 410 B2, Dec. 21, 2021.

[28] F. Laghezza and F. Lampel, "Predistortion technique for joint radar/communication systems," U.S. Patent 2021 0 341 567 A1, Nov. 4, 2021.

[29] F. Lampel, R. F. Tigrek, A. Alvarado, and F. M. J. Willems, "A performance enhancement technique for a joint FMCW radcom system," in *Proc. 16th Eur. Radar Conf.*, Oct. 2019, pp. 169–172.

[30] F. Uysal, "Phase-coded FMCW automotive radar: System design and interference mitigation," *IEEE Trans. Veh. Technol.*, vol. 69, no. 1, pp. 270–281, Jan. 2020.

[31] U. Kumbul, N. Petrov, C. S. Vaucher, and A. Yarovoy, "Receiver structures for phase modulated FMCW radars," in *Proc. 16th Eur. Conf. Antennas Propag. (EuCAP)*, Mar. 2022, pp. 1–5.

[32] U. Kumbul, N. Petrov, C. S. Vaucher, and A. Yarovoy, "Smoothed phase-coded FMCW: Waveform properties and transceiver architecture," *IEEE Trans. Aerosp. Electron. Syst.*, early access, Sep. 12, 2022, doi: 10.1109/TAES.2022.3206173.

[33] M. I. Skolnik, *Radar Handbook*. New York, NY, USA: McGraw-Hill, 2008.

[34] S. A. Elgamel, C. Clemente, and J. J. Soraghan, "Radar matched filtering using the fractional Fourier transform," in *Proc. Sensor Signal Process. Defence*, Sep. 2010, pp. 1–5.

[35] N. Petrov and A. G. Yarovoy, "Fractional Fourier transform receiver for modulated chirp waveforms," *IEEE Trans. Microw. Theory Techn.*, early access, Nov. 29, 2022, doi: 10.1109/TMTT.2022.3222225.

[36] M.-E. Chatzitheodoridi, A. Taylor, and O. Rabaste, "A mismatched filter for integrated sidelobe level minimization over a continuous Doppler shift interval," in *Proc. IEEE Radar Conf.*, Sep. 2020, pp. 1–6.

[37] N. Levanon and E. Mozeson, *Radar Signals*. New Jersey, NJ, USA: Wiley, 2004.

[38] D. R. Fuhrmann and G. S. Antonio, "Transmit beamforming for MIMO radar systems using signal cross-correlation," *IEEE Trans. Aerosp. Electron. Syst.*, vol. 44, no. 1, pp. 171–186, Jan. 2008.

[39] S. Ahmed, P. Aubry, and A. Yarovoy, "Experimental study on multi-channel waveform agile beamforming and testbed calibration," in *Proc. IEEE Conf. Antenna Meas. Appl. (CAMA)*, Nov. 2021, pp. 248–253.

Utku Kumbul (Graduate Student Member, IEEE) received the B.Sc. degree (Hons.) in electrical and electronics engineering (main major) and the second B.Sc. degree (Hons.) in computer engineering (double major) from the Department of Electrical and Electronics Engineering and the Department of Computer Engineering, Atilim University, Ankara, Turkey, in 2014 and 2015, respectively, and the M.Sc. degree in electrical and electronics engineering from the TOBB University of Economics and Technology, Ankara, in 2017. He is currently pursuing the Ph.D. degree in electrical engineering at the Delft University of Technology, Delft, The Netherlands.

From 2017 to 2018, he was a Hardware Engineer with Havelsan Ehsim, Air Electronic Warfare Systems Engineering, Inc., Ankara, where he was a part of the passive radar and decoy projects. His current research interests include waveform design, radar signal processing, interference mitigation, MIMO systems, and automotive radars.

Mr. Kumbul is a Reviewer for the IEEE TRANSACTIONS ON AEROSPACE AND ELECTRONIC SYSTEMS, the IEEE TRANSACTIONS ON MICROWAVE THEORY AND TECHNIQUES, and *IET Radar, Sonar and Navigation*.

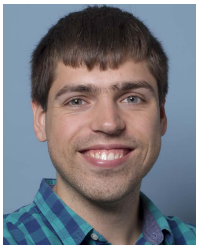

Nikita Petrov received the B.Eng. degree in radioelectronic control systems from Baltic State Technical University Voenmeh, Saint Petersburg, Russia, in 2012, and the Ph.D. degree in radar signal processing from the Delft University of Technology, Delft, The Netherlands, in 2019.

Since 2019, he has been a Post-Doctoral Researcher with the Microwave Sensing, Signals and Systems (MS3) Section, Faculty of Electrical Engineering, Mathematics, and Computer Science (EEMCS), Delft University of Technology. Since April 2022, he has been with NXP Semiconductors N.V., Eindhoven, The Netherlands, and part time with the same group at the Delft University of Technology. His research interests include modern radar technologies, radar signal processing, multichannel and multiband signals and systems, and high-resolution and automotive radars.

Dr. Petrov currently serves as a Reviewer for the IEEE TRANSACTIONS ON AEROSPACE AND ELECTRONIC SYSTEMS and the IEEE TRANSACTIONS ON GEOSCIENCE AND REMOTE SENSING.

Cicero S. Vaucher (Senior Member, IEEE) received the Ph.D. degree in electrical engineering from the University of Twente, Enschede, The Netherlands, in 2001.

He was with Philips Research Laboratories, Eindhoven, The Netherlands, from 1990 to 2006, when he joined NXP Semiconductors N.V. He is currently an Automotive Radar Product Architect with the ADAS Product Line. He is also a part-time Professor with TU Delft, where he is working on mmWave front-ends. He is the author of *Architectures for RF Frequency Synthesizers* (Boston, MA, USA: Kluwer, 2002) and is a coauthor of *Circuit Design for RF Transceivers* (Boston, MA, USA: Kluwer, 2001). He is (co-)inventor of 28 unique patent families. His research activities and interests include micro-wave and mm-Wave transceiver architectures, radar system implementation and signal processing, and implementation of circuit building blocks.

Dr. Vaucher is an NXP Technical Fellow. He was a member of the Technical Program Committee of the IEEE Custom Integrated Circuits Conference (CICC) from 2005 to 2013, acting in the wireless subcommittee. He is currently acting on the IEEE-MTT Connected and Autonomous Systems Technical Committee 27.

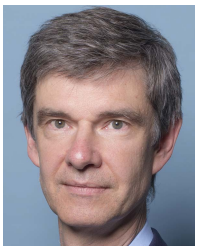

Alexander Yarovoy (Fellow, IEEE) received the diploma degree (Hons.) in radiophysics and electronics from Kharkov State University, Kharkiv, Ukraine, in 1984, and the Candidate Phys. and Math. Sci. and Doctor Phys. and Math. Sci. degrees in radiophysics, in 1987 and 1994, respectively.

In 1987, he joined the Department of Radiophysics, Kharkov State University, as a Researcher and became a Full Professor in 1997. From September 1994 to 1996, he was with the Technical University of Ilmenau, Ilmenau, Germany, as a Visiting Researcher. Since 1999, he has been with the Delft University of Technology, Delft, The Netherlands. Since 2009, he has been leading there as a Chair of microwave sensing, systems and signals. He has authored and coauthored more than 500 scientific or technical articles, seven patents, and 14 book chapters. His main research interests are in high-resolution radar, microwave imaging, and applied electromagnetics (in particular, UWB antennas).

Prof. Yarovoy was a recipient of the European Microwave Week Radar Award for the paper that best advances the state-of-the-art in radar technology in 2001 (together with L. P. Ligthart and P. van Genderen) and in 2012 (together with T. Savelyev). In 2010 together with D. Caratelli, he got the Best Paper Award of the Applied Computational Electromagnetic Society (ACES). He served as a General TPC Chair for the 2020 European Microwave Week (EuMW'20), as the Chair and a TPC chair for the 5th European Radar Conference (EuRAD'08), and the Secretary for the 1st European Radar Conference (EuRAD'04). He also served as the Co-Chair and TPC Chair for the Xth International Conference on GPR (GPR2004). He served as an Associated Editor for the *International Journal of Microwave and Wireless Technologies* from 2011 to 2018 and as a Guest Editor of five special issues for the IEEE TRANSACTIONS and other journals. From 2008 to 2017, he served as the Director for the European Microwave Association (EuMA).